

Supporting Information

Experimental data

Materials synthesis

Initially, purified natural molybdenum disulfide (DM-1, Scopin factory, Russia) with a particle size (95%) smaller than 7 μm was intercalated with lithium by treating it with an excess of 1.6 M n-butyllithium solution in hexane (Aldrich) for one week followed by washing with hexane and vacuum drying. Then, the obtained product, Li_1MoS_2 was placed in bi-distilled water, sonicated for 15 min and then stirred on a magnetic stirrer for 30 min to prepare the 1 mg mL⁻¹ aqueous dispersion of MoS_2 . Tetramethylammonium bromide (Me_4NBr) or tetraethylammonium bromide (Et_4NBr) or diethylamine (Et_2NH) taken in amount of 10 mol/mol of MoS_2 were dissolved in 20 ml of water (acidified with HCl to pH 3 in case of Et_2NH) and added to 200 ml of the dispersion. In case of Et_2NH , additional amount of HCl was added to the mixture to adjust pH to 2. The mixture was stirred for 30 min on a magnetic stirrer. The precipitate was isolated by centrifugation, washed 3 times with water and dried in vacuum. The composition of products was determined from the elemental analysis data (C, H, N, Mo).

TEM

HRTEM images were obtained on a JEM-2200FS electron microscope (JEOL Ltd. Japan), with a lattice-fringe resolution of 0.1 nm at an accelerating voltage of 200 kV. The high-resolution images of periodic structures were analyzed and filtered by the Fast Fourier Transformation (FFT) method with the help of computer software DigitalMicrograph™ 3.6.5 (Gatan Inc.). Multislice image simulation of HRTEM images has been used and their comparison to images received on an electron microscope. Electron Microscopy Software «JEMS», version: 3.3526U2008 (P.Stadelmann, CIME-EPFL) was used for simulation.

Samples to be examined by HRTEM were prepared on a perforated carbon film mounted on a copper grid.

Powder diffraction

The powder diffraction patterns of **TE** and **TM** were measured using on a Bruker D8 Advance Vario diffractometer with Ge(111) Cu $K\alpha^1$ monochromator and LynxEye 1D silicon strip detector, in transmission between Kapton films, measurement range 6-120° 2 θ step size 0.00917° 2 θ . All modeling and indexing was performed using Bruker TOPAS 4.2.¹

Indexing of the powder patterns

The peaks of the pattern, except for the 00l ones, were described as a separate peaks phases and indexing was attempted with default settings. The TOPAS software lists the two-dimensional space groups with negative volume and $c=-999$ Å. For the Pawley fit, the c parameter was set to 0.1 Å, and the unit cell parameters refined to $a=5.6991(12)$ and $b=3.2001(10)$ in TM. The actual precision of these values was limited, since the Pawley fit did not provide an adequate description of the $hk0$ zone due to problems with the peak shape. The peak asymmetry was partially described using a constant positive “circles” convolution, which does not exactly correspond to the asymmetry expected for the turbostratic disorder (Figure S1).

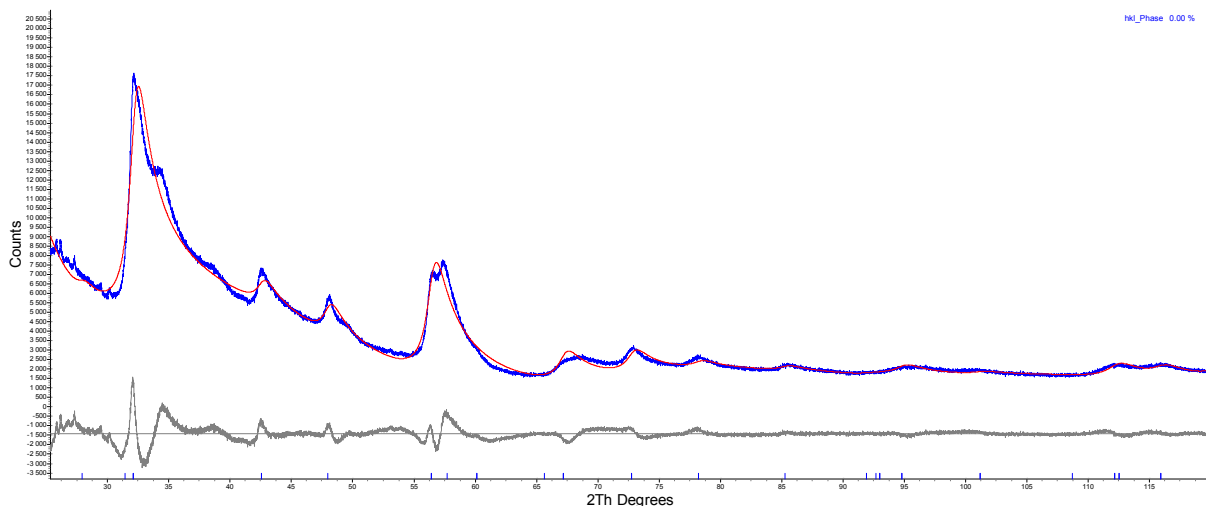


Figure S1. The Pawley fit of the hk0 reflections of TM. Red line — calculated pattern, blue — experimental one, grey — their difference.

Refinement of hexagonal model, case of TE

The TE powder pattern was refined using Ufer's approach as

The three closest Mo-Mo distances (3.57 Å, 3.20 Å, 2.95Å) approximated those known from EXAFS data² for the studied systems (3.76 Å, 3.15 Å, 2.77 Å). Half of the sulfur atoms shifted inside the layer, and half outside, forming valleys 0.32 Å deep, which matched the refined positions of cations. Unfortunately, this simple model demonstrated serious problems: while unrestrained, the shortest intralayer S...S distances reached 2.2 Å — an obviously unreasonable value. When the distance was restrained to 2.7 Å (the shortest known S...S contact for Mo complexes according to the CSD database³), the fits became quite unsatisfactory, particularly for the 210, 110 and 410 diffraction bands in the TE powder pattern (Figure S4).

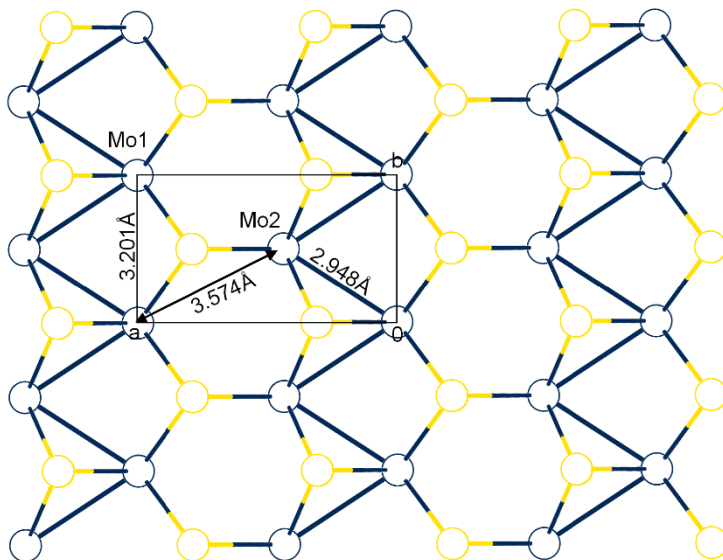


Figure S2. The MoS₂ layer structure of TE in the distorted prismatic mode, view in the *c* direction. Rectangle denotes the refined supercell, Mo-Mo distances are labeled. NEt₄ cation is omitted for clarity.

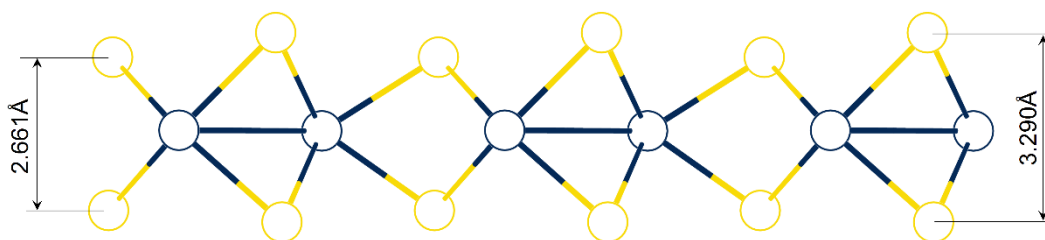


Figure S3. MoS₂ layer structure in the distorted prismatic model, view in the *b* direction.

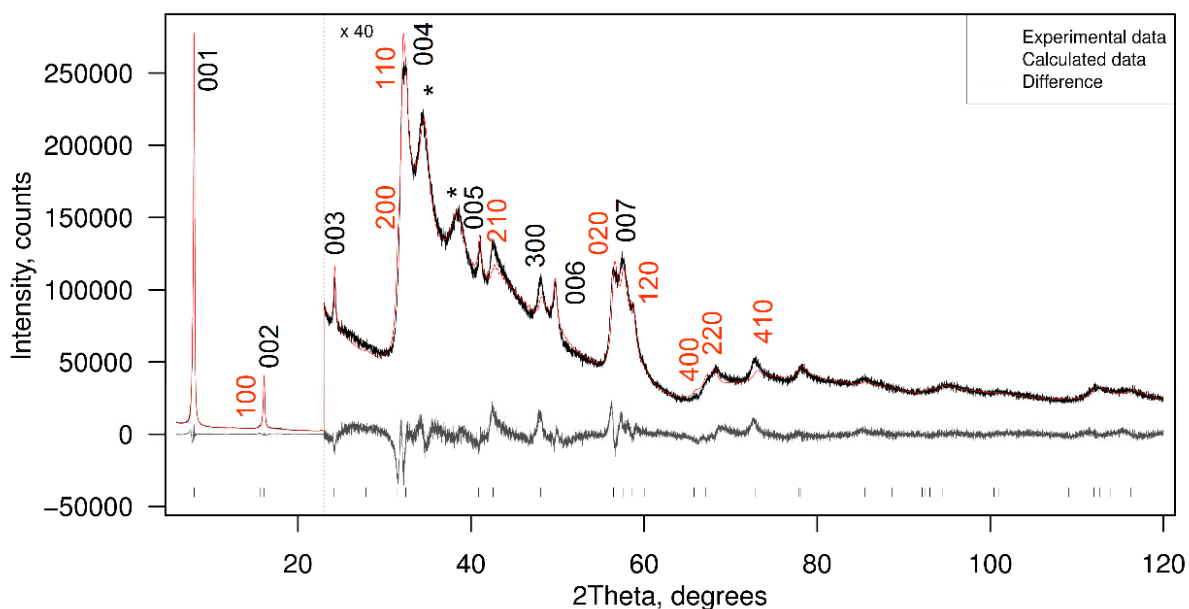


Figure S4. Powder pattern of TE refined within the distorted prismatic model. Diffraction bands are labeled in red, stars correspond to the independently refined peaks (see Refinement model), ticks label peak positions. Note the misfit of the 110, 210 and 410 reflections.

Rietveld refinement details

The refinement was performed using the Wang implementation of the K. Ufer's supercell model for TOPAS 4.2. The base unit cell represented one MoS_2 and one organic layer; no symmetry constraints were applied. We chose the factor of elongation $N=15$ for all patterns as the fit did not noticeably improve with its further increase. The discussion of the unit cell contents and coordinates in the rest of the manuscript refers to the unit cell without the multiplication in the c^* direction; the term "supercell", unless otherwise specified, refers to long-range ordering in the (ab) plane and not to the "virtual" supercell of the Ufer's model. The least-squares refinement process was identical to a normal Rietveld refinement, with reasonable refinement speed: each refinement step ran for 10-15 minutes until convergence on a 2.5 GHz processor.

The Mo-S distances were restrained to the EXAFS-derived² value of 2.4 Å. The precise position of the cations was obtained by the refinement with anti-bump restraints on S...C

contacts (minimum value of 3.4 Å). The cations were refined as rigid bodies, with occupancy set from chemical analysis data. As the unit cell had $Z=2$, the occupancy was set to 0.5 for Me_4N^+ and to 0.32 for Et_4N^+ and H_2NEt_2^+ . The optimal cation position was found with help of the anti-bump restraints by limited simulated annealing. The found minima was indicated by a sharp decrease of the average U_{iso} for the cation and a drop in overall R_{wp} . The cations remained in place after the removal of anti-bump restraints. The rotations around C-N bonds were not refined.

The line broadening was dominated by strain-like contributions (dependent on ϵ), indicating significant unit-cell parameter variation across the crystallites and/or presence of large amount of defects. Both patterns exhibited preferred orientation effects, consistent with orientation of plate-like crystallites perpendicular to the X-ray beam. The factor for scaling the 00l reflections, theoretically 15, refined to 2.01(2) for **TM**, 11.09(10) for **TE** and 6.39(7) for **DE**. Formula (1), where ϵ_{hkl} is a free parameter, and a, b, c refer to the parameters of the virtual supercell, was used on peaks with $h \neq 0$ or $k \neq 0$ to avoid “ripples”.

$$FWHM_{hkl} = \sqrt{(\epsilon_{hkl} \tan \theta)^2 + \frac{l^2}{c^2 l^2 + c^4 \left(\frac{h^2}{a^2} + \frac{k^2}{b^2} \right)}} \quad (1)$$

Studied powder patterns contain symmetric low-intensity wide peaks at $34.51(1)^\circ$ and $38.60(1)^\circ$ 2θ , which cannot be indexed within any reasonable supercell. Moreover, the peak shape indicates that they cannot correspond to the $hk0$ family of reflections. We assume that these peaks correspond to the long-range interlayer positional correlations, and refined these two peaks as a peak phase to stabilize the overall refinement. The **TM** pattern contained small sharp peaks most likely corresponding to organic impurities in the sample.

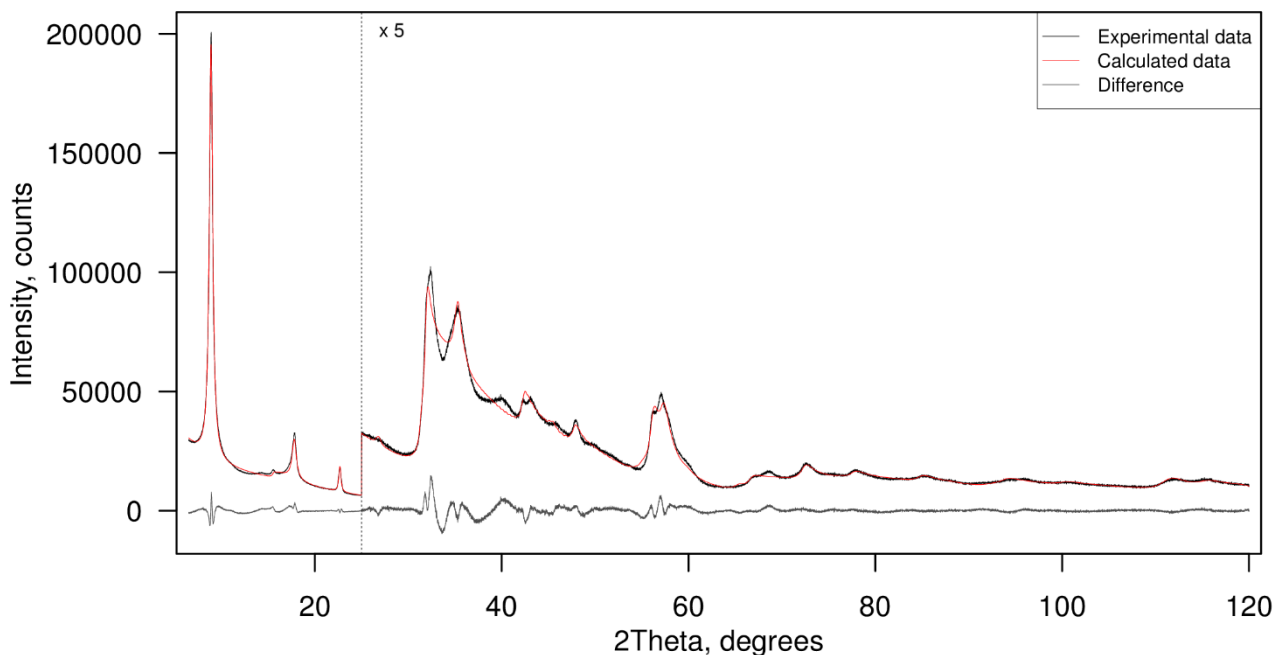


Figure S5. The fit of DE powder pattern.

Periodic DFT calculations

The model was constructed basing on the TE structure using only the $[X+1, Y+1, Z]$ operation to fit the cation rows together and ignoring the turbostratic disorder. This structure is obviously not dominant in the actual TE, but the turbostratic disorder means that all relative positions of layers have approximately equivalent energies, and the absence of this structure is dictated mostly by entropic factors.

This opens a possibility for a straightforward periodic DFT calculation not taking the interlayer disorder into account; in any case, the turbostratic disorder suggests that all relative orientations of the layers are possible, so we chose the simplest for the calculation, assuming an ordered 3-dimensional structure without any relative rotation of the layers.

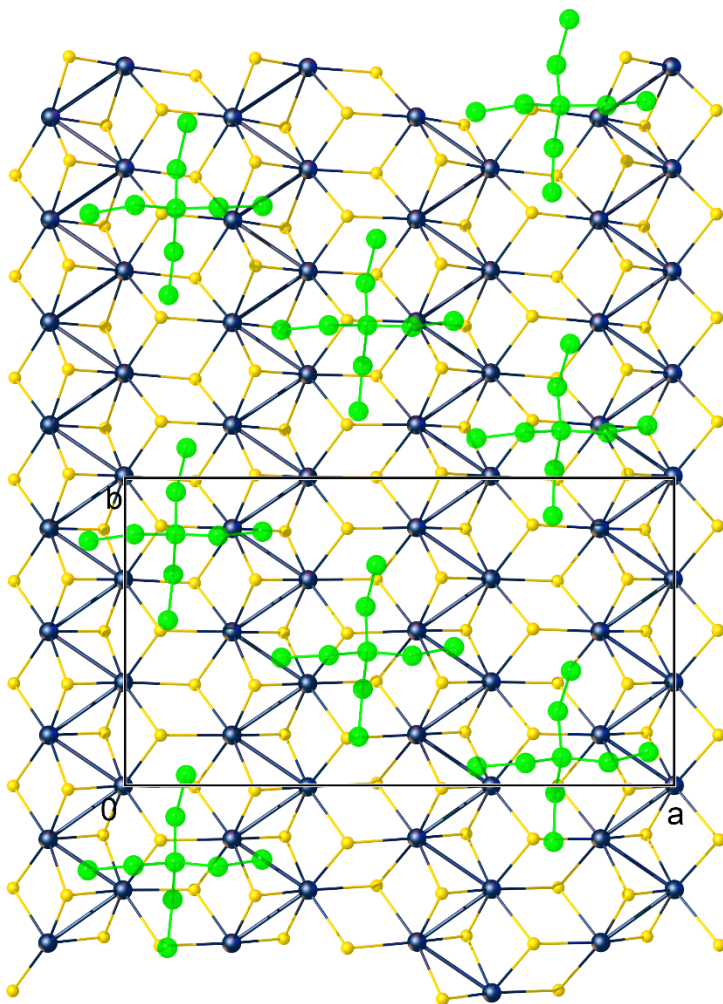


Figure S6. The calculated layer structure of TE. Hydrogen atoms are omitted, the TE cations are denoted in green.

The calculation of TE was performed in VASP⁴⁻⁷ in the simplified “ordered” model (without interlayer rotation), using a 3*3*1 supercell basing on the experimental one. Simultaneous optimization of all atomic positions starting from experimental coordinates diverged; thus the optimization was performed in two steps, first by molecular dynamics modeling of the organic layer with frozen MoS₂ one, and then by the optimization of the model as a whole. The rotation of the ethyl groups of the cation resolved all shortened intermolecular contacts. Conjugated gradient technique was used for optimizations of the atomic positions and minimization of total energy. Projected augmented wave (PAW) method was applied to account for core electrons while valence electrons were

approximated by plane-wave expansion with 400 eV cutoff. Exchange and correlation terms of total energy were described by PBE exchange-correlation functional.⁸ Kohn-Sham equations were integrated using Γ -point approximation. At a final step of our calculations atomic displacements converged better than $0.01 \text{ eV}\cdot\text{\AA}^{-1}$, as well as energy variations were less than 10^{-4} eV .

The final geometry was obtained with energy cutoff of 545 eV, “hard” pseudopotentials for all atoms, using a PBE functional with Grimme VdW corrections, converging with forces less than 0.01 a.u on each atom. The calculated coordinates, formatted SHELX-style, can be found in supporting information file **calc_TE_ordered_res.txt**. In order to perform the topological analysis the electron density distribution functions were calculated on dense FFT (fast Fourier transformation) grid $560 \times 320 \times 336$, with energy cutoff of 1000 eV. The topological analysis was carried out by AIM program (part of ABINIT software⁹).

Electron microscopy

Figure S7 shows the image of a hexagonal MoS_2 particle found in the TEM data, most likely formed under the electron beam (since the XRD patterns show no 2H- MoS_2 impurities in the sample).

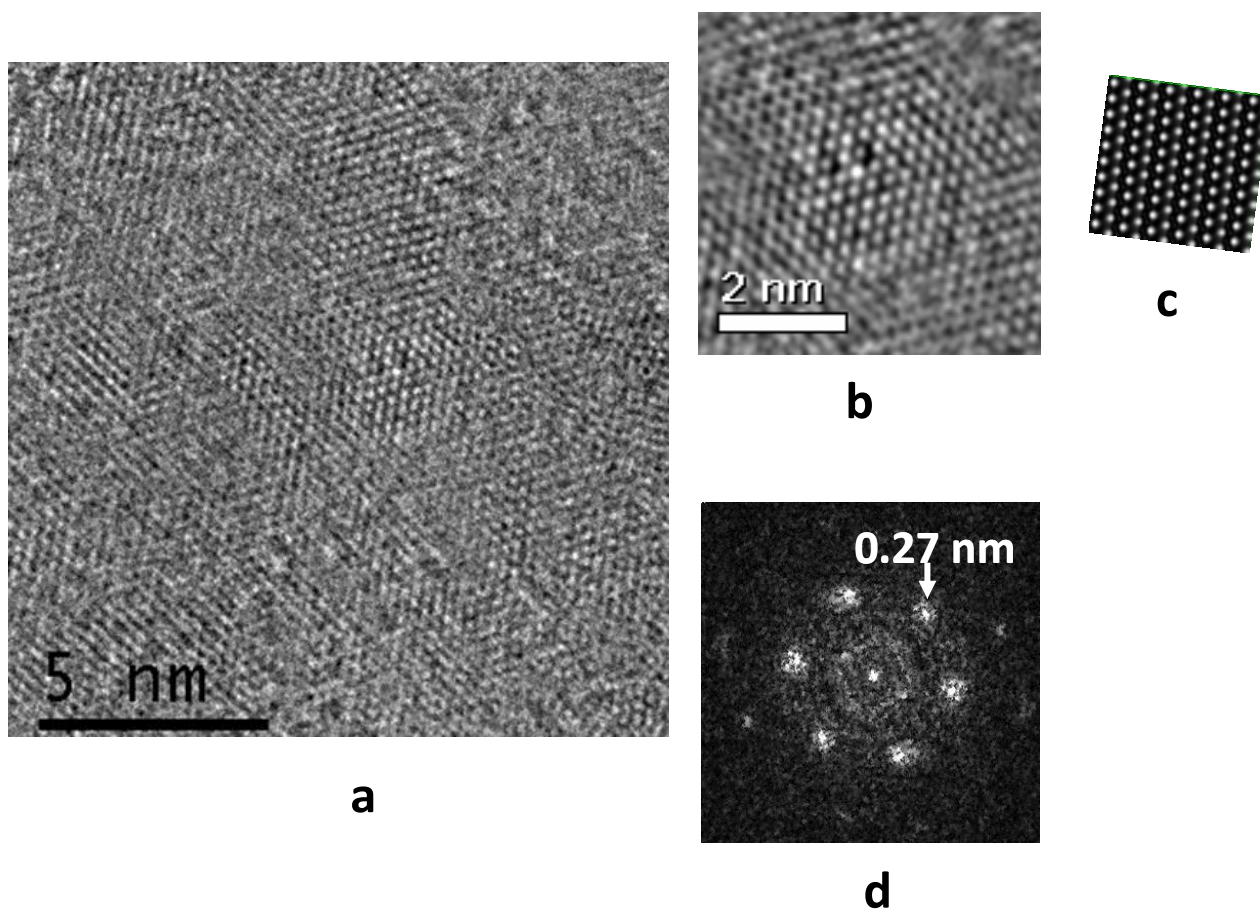


Figure S7. The HRTEM image of a hexagonal particle in basal projection (a), its magnified fragment (b) and contrast function (c) (modeling parameters: lens defocussing of 63.0 nm, crystal thickness of 29.8 nm, single-layer 2H- MoS_2 used to model) and its FFT from all area of “a” (the reflection from lattice parameter $d_{100} = 0.27$ nm is shown) (d).

- (1) Bruker. *TOPAS 4.2 User Manual*; Bruker AXS GmbH: Karlsruhe, Germany, 2009.
- (2) Zubavichus, Y. V.; Golub, A. S.; Lenenko, N. D.; Novikov, Y. N.; Slovokhotov, Y. L.; Danot, M. *Journal of Molecular Catalysis A: Chemical* **2000**, *158*, 231–236.
- (3) Allen, F. *Acta Cryst. Sect. B* **2002**, *58*, 380–388.

- (4) Kresse, G.; Hafner, J. *Phys. Rev. B* **1994**, *49*, 14251–14269.
- (5) Kresse, G.; Hafner, J. *Phys. Rev. B* **1993**, *47*, 558–561.
- (6) Kresse, G.; Furthmüller, J. *Phys. Rev. B* **1996**, *54*, 11169–11186.
- (7) Kresse, G.; Furthmüller, J. *Comput. Mater. Sci.* **1996**, *6*, 15–50.
- (8) Perdew, J. P.; Burke, K.; Ernzerhof, M. *Phys. Rev. Lett.* **1996**, *77*, 3865.
- (9) Gonze, X.; Beuken, J.-M.; Caracas, R.; Detraux, F.; Fuchs, M.; Rignanese, G.-M.; Sindic, L.; Verstraete, M.; Zerah, G.; Jollet, F.; Torrent, M.; Roy, A.; Mikami, M.; Ghosez, P.; Raty, J.-Y.; Allan, D. C. *Comput. Mater. Sci.* **2002**, *25*, 478–492.